

# TRIUMF Neutral Atom Trap (TRINAT) for Beta Decay

Work Term Report:  
Upgrading to Liquid Crystal Binary Rotator and Blackfly-S Camera

Lina Nguyen  
April 30, 2019

# Contents

1. Introduction
  - i. Experiment Overview
  - ii. Motivation for Improved Circular Polarization
2. Circular Polarization
  - i. Stokes' Formalism
  - ii. Mueller Matrices
  - iii. Quarter Wave Plates
  - vi. Measuring S3
3. Characterization of First Liquid Crystal Binary Rotator
  - i. Manufacturer's Specifications
  - ii. Polarization Axis
  - iii. 90 Degree Flip
  - iv. Flipping Time
  - v. S3 and Discussion
4. Characterization of Second Binary Rotator
  - i. Polarization Axis
  - ii. 90 Degree Flip
  - iii. S3 and Discussion
  - Iv. Replacement Rotator
5. Camera Programming
  - i. Dynamic Memory Allocation
  - ii. Achieving Maximum Frame Rate
  - iii. Information From PointGrey
6. Looking Forward
7. References

## Figures

### 1. Introduction

#### i. Experiment Overview

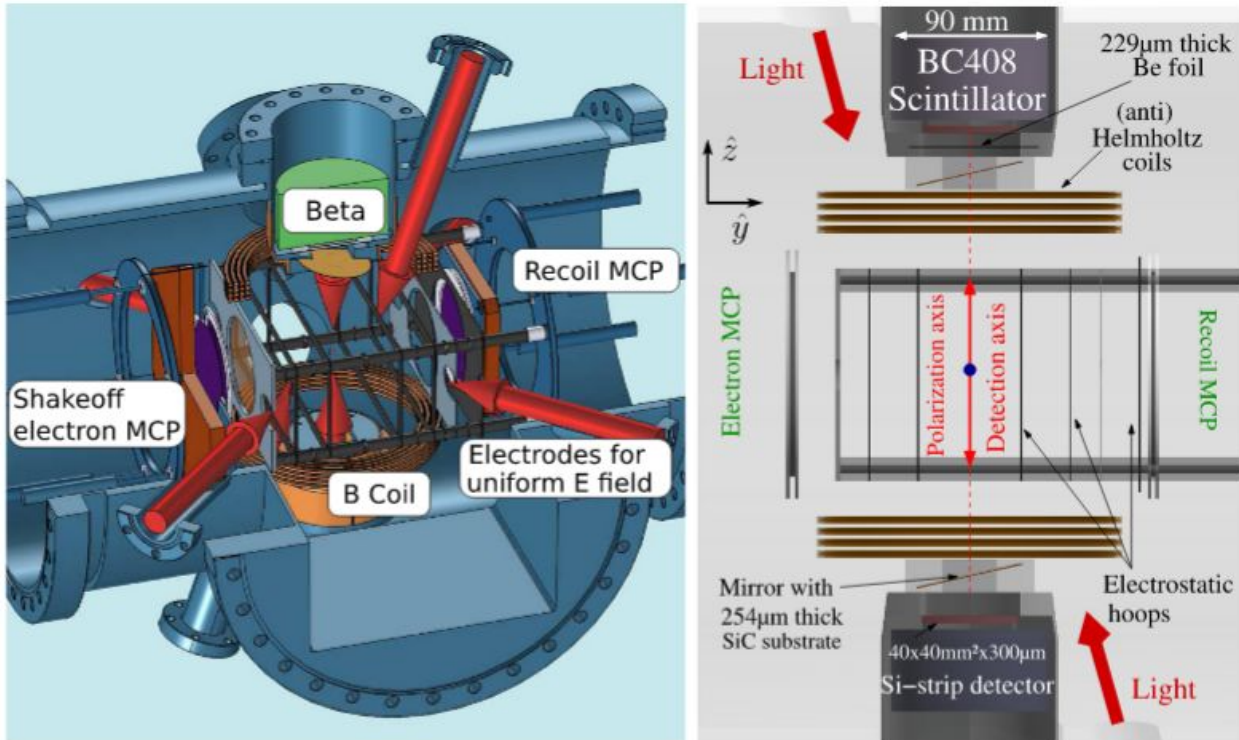
TRIUMF's Neutral Atom Trap for Beta Decays (TRINAT) studies weak interactions by observing beta decays of various elements, particularly the decays of potassium 37 into other

particles, including neutrinos and beta particles. The goal is to measure the Beta asymmetry angular correlation parameter to a precision of 0.1% in order to be competitive in the search for new physics possibly beyond the standard model.

Beta decays are studied by trapping and polarizing atoms. First, potassium 37 ions, coming from ISAC, are neutralized and gathered in the first magneto-optical trap. Then, a red detuned laser collects the atoms into the main magneto-optical trap, used for precision measurement. In the main magneto-optical trap, a process called 'optical molasses', in which pairs of laser light along each axis hit the atoms, confines the atoms to the center of the trap. Photons from the laser light impart their momentum to the atoms, and due to the doppler effect, atoms absorb more momentum if they are travelling towards the incident beam. As such, they slow down. Additionally, anti-Helmholtz coils are used to extinguish the magnetic field at the center, thus producing a linear restoring force constraining atoms to the center. Another static B field is applied to break degeneracy of the Zeeman sublevels as well. Outside the trap, near-Helmholtz coils are also used to counteract the magnetic field of the earth and the cyclotron. Essentially, the magneto-optical trap (MOT) confines and cools the neutral potassium 37 atoms while optical pumping spin-polarizes them.

After the atoms are trapped, the MOT is turned off and laser light is used to optically pump the atoms, making them highly polarized. Polarizing the atoms lends to the prediction of the recoiling nuclei coming from the decay. The MOT is turned off because the trap destroys any polarization. The degree of nuclear spin polarization is measured by monitoring the total  $P_{1/2}$  population of the atoms. The population is directly related to the degree of polarized atoms as fully polarized atoms are in the ground state,  $S_{1/2}$ , and are not excited by the optical pumping light. The  $P_{1/2}$  population is monitored by detecting fluorescent light emitted as atoms de-excite to the  $S_{1/2}$  state. As such, less fluorescent light indicates a higher degree of polarization. The degree of polarization approaches unity after approximately 100us of optical pumping.

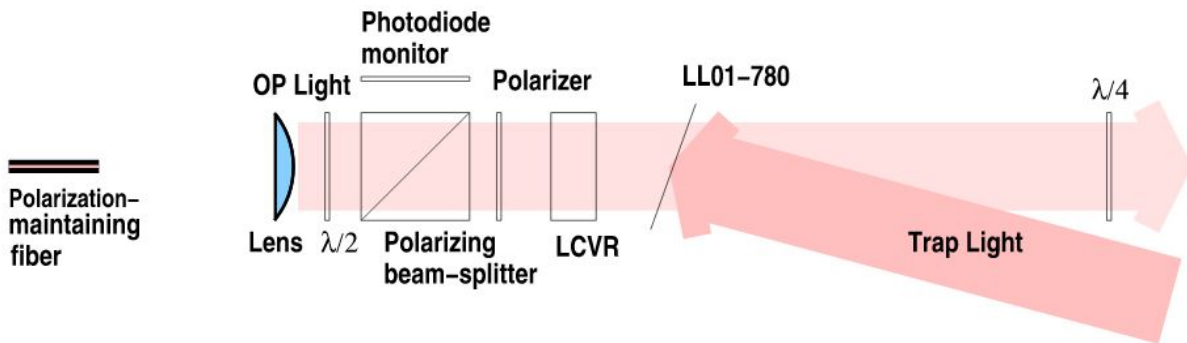
The experimental setup for TRINAT's beta decay experiments is as follows:



$\vec{a} \sim \frac{1}{\hbar} \int \vec{E}(\vec{r}, t) dt$

The silicon strip detector and scintillator define the polarization axis. Individually, the silicon strip detector eliminates background signals and provides positron information while the scintillator stops positrons coming from the detector. The electrostatic hoops maintain a uniform electric field. On the left, the red arrows are the MOT's laser beams, while on the right, the arrows represent the optical pumping beams entering at  $9.5^\circ$  to the normal. Utilising two symmetric detectors and regularly flipping the sign of the optical pumping light minimizes systematic uncertainty.

Below is the setup for the optical pumping light beams:



~~0a ~ !^AGU^c] Á Á@Á] 2aÁ ~ { ] ă \* Á@ Á^æ • ÉÁ~~

The half-wave plate, polarizing beamsplitter, and photodiode combination realigns the incoming optical fibre beam polarization axis with the vertical. The beamsplitter is adjusted until the photodiode signal is minimized, thus maximizing the light intensity leaving the beamsplitter. The polarizer then ensures well polarized light incident on the rotator, which periodically flips the linearly polarized light between two states 90 degrees apart. This alternation is responsible for the periodic sign flip of the circular polarization needed to reduce systematic uncertainties in the recorded beta decay rates. The quarter wave plate turns the linear polarization into either left or right circular polarization depending on the state of the rotator. The Semrock filter aligns the magneto-optical trap light with the optical pumping light.

In this work term, the goal is to investigate the performance of a new apparatus, the liquid crystal binary rotator, which acts in the place of the liquid crystal variable retarder to change the sign of the circular polarization. The liquid crystal binary rotator is expected to improve the resulting circular polarization, which is also to be measured.

## ii. Motivation for Improved Circular Polarization

The beta asymmetry is calculated as follows:

$$A_{\beta} = \frac{A_{\text{obs}}}{P} = \frac{1}{P} \frac{r^{\uparrow} - r^{\downarrow}}{r^{\uparrow} + r^{\downarrow}}$$

~~0a ~ !^AGU^c] Á Á@Á] 2aÁ ~ { ] ă \* Á@ Á^æ • ÉÁ~~

Here,  $A_{\text{obs}}$  is the observed beta asymmetry, which is the difference between the two beta particle count rates observed on the two detectors divided by the total count rate while  $P$  is the nuclear polarization of the atoms.  $r^{\uparrow}$  and  $r^{\downarrow}$  are the number of beta particles hitting the top detector and the bottom detector respectively. The systematic uncertainty of the beta asymmetry value is ultimately dependent on our systematic uncertainty on the nuclear polarization. In turn, the uncertainty in the nuclear polarization is dependent on the uncertainty of the circular polarization. Any component of light with the 'wrong' polarization will remove atoms from the fully polarized state, ie. it will cause  $|P| < 1$ . On the other hand, with less unpolarized light, there will be less uncertainty on the nuclear polarization and alignment.

In particular, the motivation for the liquid crystal binary rotator to replace the liquid crystal variable retarder is to improve the final circular polarization. The error in the circular polarization is third largest contribution to the systematic uncertainty, and is arguably the most 'fixable' one. For instance, the new binary rotator has a specification for extinction at least 2.5x better than the variable retarder. It can be up to 5x better than the variable retarder in its extinction when used in conjunction with a good polarizer.

## 2. Circular Polarization

### i. Stokes' Formalism

This section summarizes the information found in [6]. If the z direction is taken to be the direction of propagation, then any polarized beam of light can be described by the general wavefunction:

$$\Psi = E_x e^{i(\omega t + \delta_1)} \hat{x} + E_y e^{i(\omega t + \delta_2)} \hat{y}$$

When the amplitudes,  $E_x$  and  $E_y$  are consistent and the phase difference is  $\pm\pi/2$ , then the light is circularly polarized. When the phase difference is 0, then the light is linearly polarized. Finally, when the amplitudes differ and the phase difference is not a multiple of  $\pm\pi/2$ , then the light is elliptically polarized.

Light beams can also be represented by density matrices. For systems which are superpositions of two orthogonal states, the density matrix is:

$$\rho = \begin{bmatrix} a_1 a_1^* & a_1 a_2^* \\ a_2 a_1^* & a_2 a_2^* \end{bmatrix}$$

The diagonal values are the 'populations;' They are the expectation values for the number of photons in each of the respective states  $a_1$  and  $a_2$ . The expectation value is the product of the wavefunction and its conjugate. On the other hand, the off-diagonals are the 'coherences' and they describe the constant, relative phase difference between the two states.

Unpolarized light can also be described by density matrices. With unpolarized light, the coherences average out to zero since there is no constant phase difference. For completely unpolarized light, the populations are equal. A beam of arbitrary polarization can be described as the superposition of completely unpolarized and completely polarized light, with coefficient 'P' signifying the degree of polarization of the light. Note that 'P' here, degree of light polarization is different than 'P' in Figure 3, degree of nuclear spin polarization. As such, the general density matrix for a beam of arbitrary polarization is:

$$\rho = P \begin{bmatrix} a_1 a_1^* & a_1 a_2^* \\ a_2 a_1^* & a_2 a_2^* \end{bmatrix} + \frac{1}{2}(1 - P) \begin{bmatrix} 1 & 0 \\ 0 & 1 \end{bmatrix} = \begin{bmatrix} \rho_{11} & \rho_{12} \\ \rho_{21} & \rho_{22} \end{bmatrix}$$

The Stokes parameters presents the information contained in a density matrix in observables. The parameters,  $S_0$ ,  $S_1$ ,  $S_2$ , and  $S_3$  respectively represent the total intensity, the

degree of plane polarization (intensity) along two arbitrary orthogonal axes, the degree of plane polarization (intensity) along orthogonal axes 45 degrees to the previous, and the degree of circular polarization. In terms of the density matrix elements, the Stokes parameters are:

$$\begin{aligned} S_0 &= p_{11} + p_{22} \\ S_1 &= p_{11} - p_{22} \\ S_2 &= p_{12} + p_{21} \\ S_3 &= \sqrt{p_{21} - p_{12}} \end{aligned}$$

$S_1$  and  $S_2$  can be measured with a polarizer, however, measuring  $S_3$  directly requires the use of a quarter wave plate which turns the circular polarization into linear polarization to be subsequently measured with a polarizer. Alternatively,  $S_3$  can be calculated knowing the values of  $S_1$  and  $S_2$ , which is the method employed in this paper. The normalized formula for  $S_1$  is:

$$S_1 = \frac{S_1}{S_0} = \frac{I_x - I_y}{I_x + I_y}$$

$S_2$  is calculated in the same way, but with the intensities along the 45 and -45 degree axes instead.

The Stokes vector is sufficient to fully characterize a beam of light. For example, a circularly polarized beam can be represented as  $[S_0; S_1; S_2; S_3] = [1; 0; 0; 1]$ . Likewise, a beam of elliptically polarized light with its maximum intensity along the x axis can be represented as  $[S_0; S_1; S_2; S_3] = [1; S_1; 0; S_3]$ . Again, light partially polarized can be represented as the sum of perfectly polarized light and perfectly unpolarized light:

$$I_{real} = I_{Polarized} + I_{Unpolarized} = P \begin{bmatrix} 1 \\ S_1 \\ S_2 \\ S_3 \end{bmatrix} + (1 - P) \begin{bmatrix} 1 \\ 0 \\ 0 \\ 0 \end{bmatrix} = \begin{bmatrix} 1 \\ PS_1 \\ PS_2 \\ PS_3 \end{bmatrix}$$

where 'P' is the degree of polarization of the light.

## ii. Mueller Matrices

Optical elements act on light beams, consequently changing one Stokes vector into another. As such, they can be represented by 4x4 matrices called Mueller matrices. Mueller matrices for various optical elements can easily be found in literature. For instance, the mueller matrix for a perfect linear polarizer in the x direction is can be represented as:

$$M_{perfect} = \frac{1}{2} \begin{bmatrix} 1 & 1 & 0 & 0 \\ 1 & 1 & 0 & 0 \\ 0 & 0 & 0 & 0 \\ 0 & 0 & 0 & 0 \end{bmatrix}$$

### iii. Quarter Wave Plates

Wave plates are retarders; they change the polarization of incident light by causing one constituent state to lag in phase behind the other by a predetermined amount. In quarter wave plates, this amount is odd multiples of  $\pi/2$ . In uniaxial birefringent mediums, wave plates have an optical axis parallel to the surface of the plate. Incident light, with its orthogonal constituents, come in either parallel to or perpendicular to this axis. The medium has two different indices of refraction in the optical axis and the axis orthogonal to it.  $n_o$  and  $n_e$  are the ordinary and extraordinary indices of refraction of the two axes respectively. The optical path difference between these constituents is:

$$\Lambda = d ( | n_o - n_e | )$$

where 'd' is the thickness of the plate. For a quarter wave plate:

$$\Lambda = (4m+1) \lambda_0 / 4$$

where 'm' is an integer. Wave plates induce a phase difference of:

$$\Delta\Phi = 2\pi/\lambda_0 \Lambda$$

Plugging the quarter wave plate value of  $\Lambda$  into the above equation, the result is a phase difference of  $(4m+1)\pi$ . Perfectly linearly polarized light entering a quarter wave plate emerges as circularly polarized light while circularly polarized light entering a quarter wave plate emerges as linearly polarized light.

The following Mueller matrix was used to predict S3 values based on extinction ratios. The Mueller matrix also allows predictions of S3 values at angles other than 45 degrees:

$$\begin{pmatrix} 1 & 0 & 0 & 0 \\ 0 & \cos^2(2\theta) & \frac{1}{2}\sin(4\theta) & -\sin(2\theta) \\ 0 & \frac{1}{2}\sin(4\theta) & \sin^2(2\theta) & \cos(2\theta) \\ 0 & \sin(2\theta) & -\cos(2\theta) & 0 \end{pmatrix}$$

### iv. Measuring S3

For a polarized beam of light, that is, when  $P=1$ , the following formula holds:



$$S_0^2 = S_1^2 + S_2^2 + S_3^2$$

Rearranging that, S3 can be found by measuring  $\dot{U}_{j\bar{a}}$  and doing the following calculation, where

$$\dot{U}_{j\bar{a}} = S_1^2 + S_2^2.$$

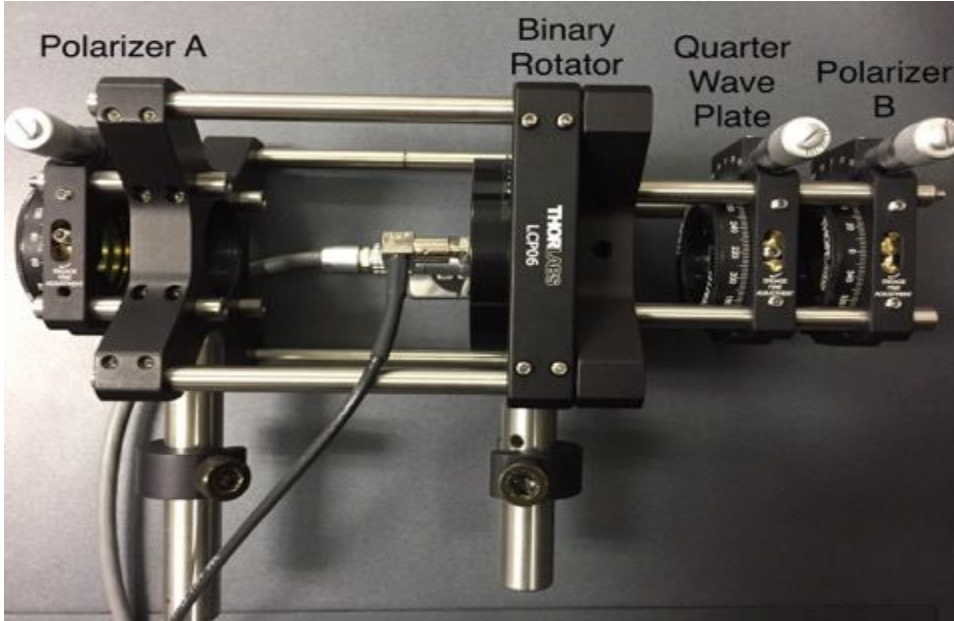
$$S_3 = \sqrt{1 - S_{lin}^2}$$

In Michael Groves' (2001) report, he uses the above formula to calculate S3. However, he says  $\dot{U}_{j\bar{a}} = P$  and defines P as:

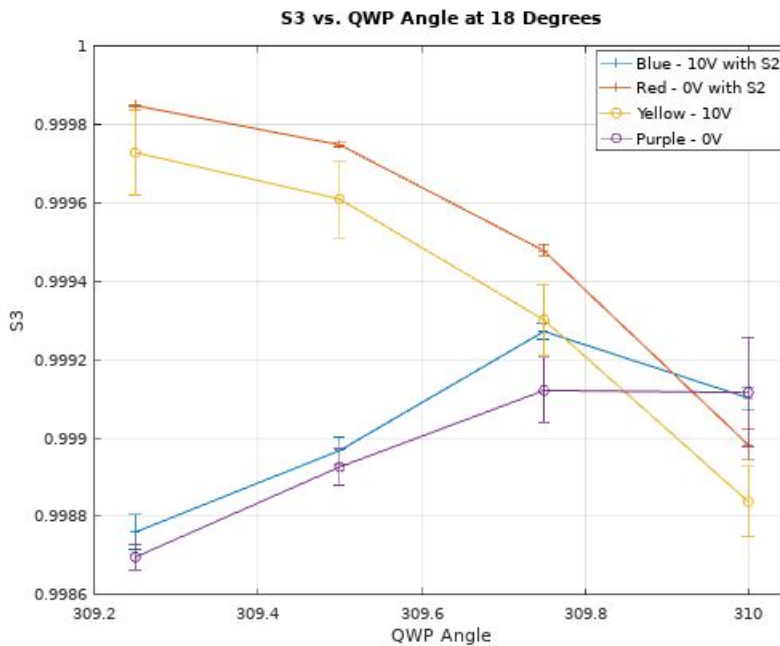
$$P = \frac{I_{max} - I_{min}}{I_{max} + I_{min}}$$

This is an incorrect assertion because in order to use the relation  $S_0^2 = S_1^2 + S_2^2 + S_3^2$ , one has to assume P=1 to begin with. In Ioana Craiciu's (2013) report, she clarifies that P=1 and  $\dot{U}_{j\bar{a}} = S_1^2 + S_2^2$ . However, she claims that if S<sub>1</sub> is taken to be (Q,  $\dot{E}Q$ ,  $\dot{D}AQ$ ,  $\dot{E}Q$ ,  $\dot{D}A$ ) then S<sub>2</sub>=0.

Experimentally, S<sub>2</sub> is not zero, even when S<sub>1</sub> is defined to be (Q,  $\dot{E}Q$ ,  $\dot{D}AQ$ ,  $\dot{E}Q$ ,  $\dot{D}A$ ). One method of measuring S3 is to measure S1 along an arbitrary set of orthogonal axes and then to measure S2 along axes 45 degrees from that. For example, S1 could be measured using the 0 and 90 degree axes, and S2 could be measured along the 45 and 135 degree axes. Another method of measuring S3 is choosing S1 to be measured along the maximum and minimum axes, then measuring S2 45 degrees from these axes. The first method is more lenient and thus yields a higher S3. Using the second method, the S2 was experimentally determined to be about 0.006 ± 0.002. The S2 contribution is negligible in the S3 calculation. As such, Michael Groves' method for calculating S3 remains sufficient, despite his incorrect assumptions.

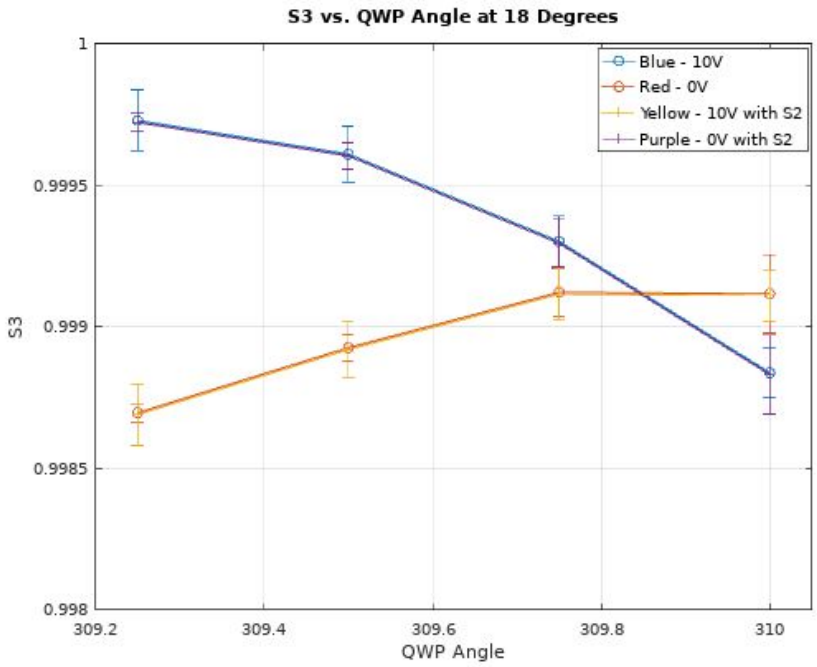


0a ~ !^A E0c / ^i q ^ } a p ^ c ] A @ , q \* A U [ | a a ^ i / O E A @ A q a s ^ A [ a e | E c @ A ~ a c ^ A a e ^ A | a e E A  
 a a A U [ | a a ^ i / O E V @ A e ^ i / A a e ^ i ^ A [ { A ^ o A A a @ a Q ~ \* Q @ A q ] a e e ^ E U [ | a a ^ i / O E A | | c a ^ A  
 \* [ [ a A q & { q \* A [ | a a a e } A A c @ A [ a e | A @ A U [ | a a ^ i / O E A ^ a A } | A i A a q \* A ^ a e ^ i ^ A } o A  
 a a A [ ] a A q & ~ a a A q A c @ A e c a A ] a e A ~ { } q \* A ^ a e E A



0a ~ !^A E U H & ~ i c ^ A e a s ~ | a e a A a a U G A q } \* A a a a e ^ A q \* | ^ A A U [ | a a ^ i / O A A A ^ \* i ^ A ^ A q a o A  
 Q E D A | | a a A a U H & ~ i c ^ A e a s ~ | a e a A a a Q } | A q A q a A a e s c } ^ a A Q E D V @ A q ^ , A ^ c Q a A  
 [ A e a s ~ | a e a \* A U H a a a A c @ A U H q E C E a a e ^ A q \* | ^ A A A ^ \* i ^ A ^ A q a o a e A q \* | ^ A & Q ^ A } A c a A

© 2014 [Redacted] | All rights reserved. This document is the property of [Redacted] and is intended for internal use only. It contains confidential information and is not to be distributed outside the organization. Any unauthorized use or disclosure is strictly prohibited. For more information, please contact [Redacted].



© 2014 [Redacted] | All rights reserved. This document is the property of [Redacted] and is intended for internal use only. It contains confidential information and is not to be distributed outside the organization. Any unauthorized use or disclosure is strictly prohibited. For more information, please contact [Redacted].

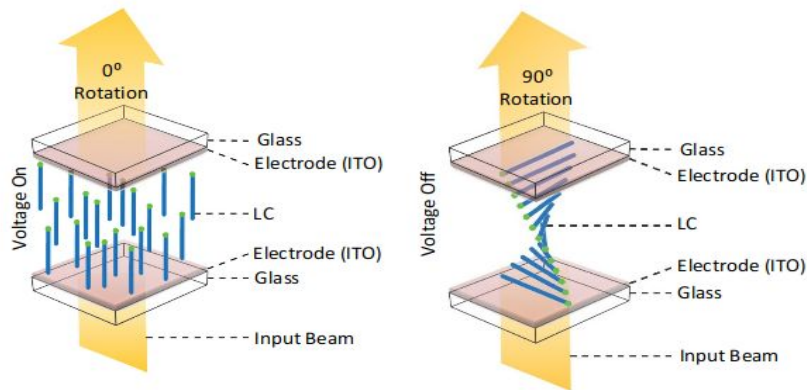
To find the S3, the fast axis was found for both the 0V and 10V beams. First, the extinction for each beam was minimized without the quarter wave plate. Then, the quarter wave plate was put between the rotator and the second polarizer and adjusted to maintain the extinction. The angle of the quarter wave plate in this orientation was taken to be the fast axis. After finding both fast axis angles, angles around the middle angle were investigated to find the optimum S3. If the flip is 90 degrees, then the fast axes are 90 degrees apart, and the middle angle would be 45 degrees away from both axes.

### 3. Characterization of First Liquid Crystal Binary Rotator

#### i. Manufacturer's Specifications

The new apparatus being tested is Meadowlark's twisted nematic liquid crystal-based binary liquid crystal rotator LTN-200. The rotator is a two-state device that rapidly flips light between two orthogonal states of linear polarization. When a voltage of 10V is applied, the emerging light has a polarization parallel to the incident light. The manufacturer states that the product is high speed, produces high purity linear polarized output, and can achieve an extinction ratio of 10,000:1 over the visible wavelength spectrum when used with a high-quality

polarizer. The rotator also has a broad temperature range, operating at up to 60 degrees Celsius.



0° Rotation

SPECIFICATIONS	
Retarder Material	Twisted Nematic liquid crystal
Substrate Material	Optical quality synthetic fused silica
Wavelength Range	400 – 1800 nm (please specify)
Transmitted Wavefront Distortion	$\lambda/4$ (P-V @ 633) $\lambda/16$ (RMS @ 633)
Response Time (vis)	$\leq 5$ ms
Surface Quality	40 – 20 scratch-dig
Beam Deviation	2 arc min
Reflectance (per surface)	0.5% at normal incidence
Diameter Tolerance	$\pm 0.10$ in.
Temperature Range	10°C to 60°C (Operating) -40°C to 90°C (Storage)
Laser Damage Threshold	500 W/cm <sup>2</sup> , CW 300 mJ/cm <sup>2</sup> , 10 ns, visible

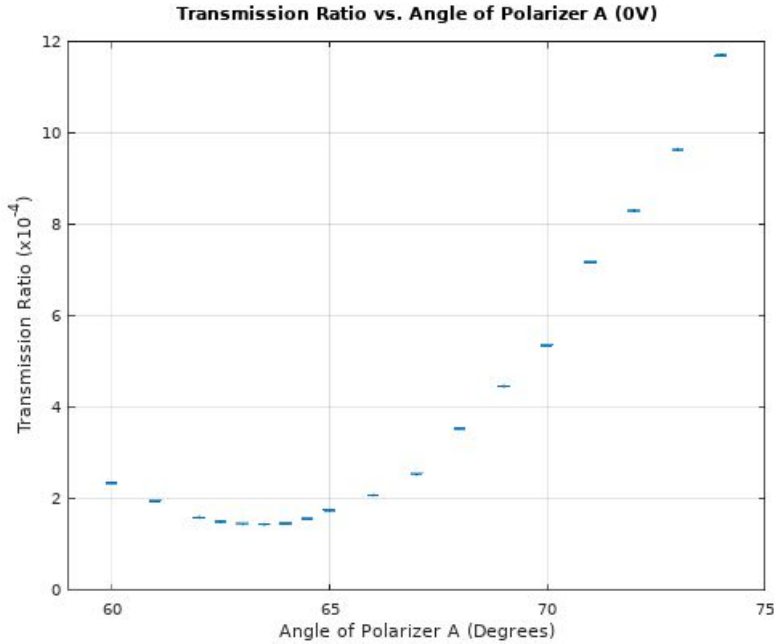
90° Rotation

## ii. Polarization Axis

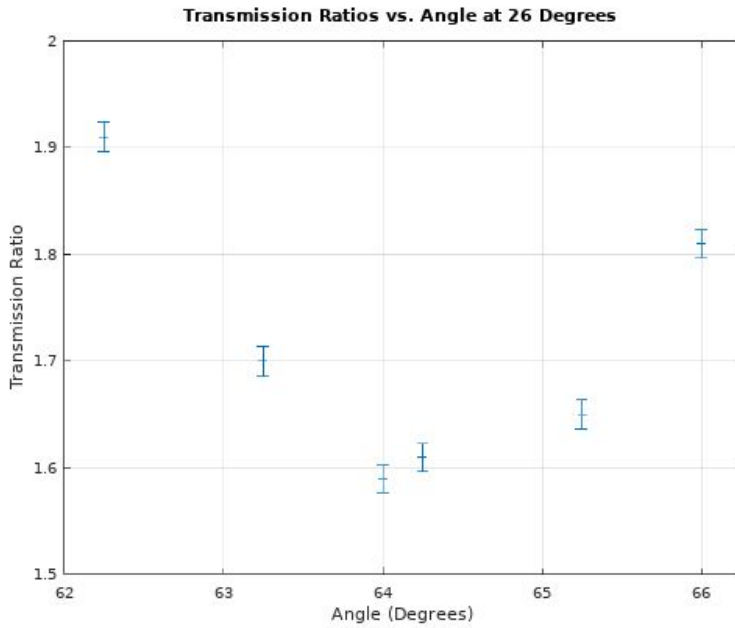
The indicated axis of the rotator was aligned vertically in the mount by using the edge of a ruler as a guide. The axis of incoming light was not well-defined. As such, the most ideal axis of the

rotator was taken to be the angle of Polarizer A (Pol A) at which the extinction ratio (maximum extinction divided by maximum transmission) was minimized.

At 24 degrees Celsius, the following trend was observed:

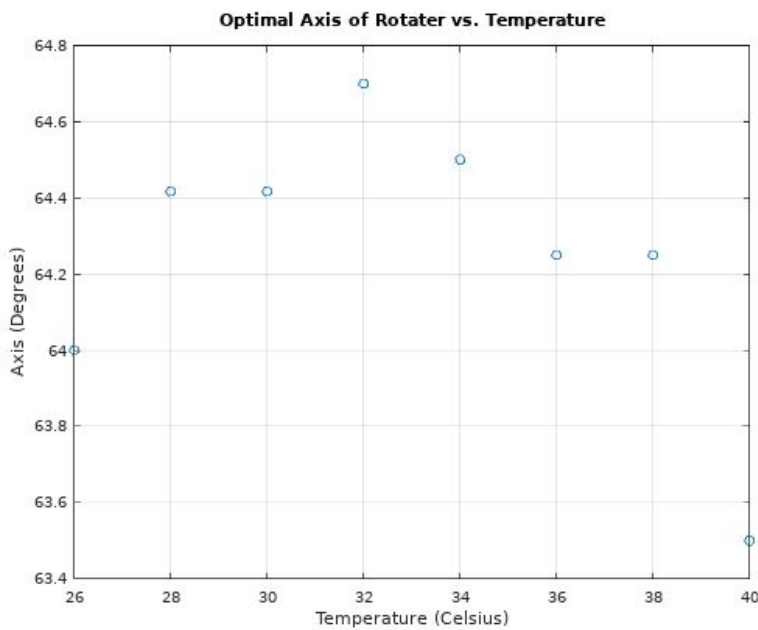


The ideal polarization axis changes with temperature. At 26 degrees, the minimum transmission and therefore axis is at 64 degrees based on the raw data:



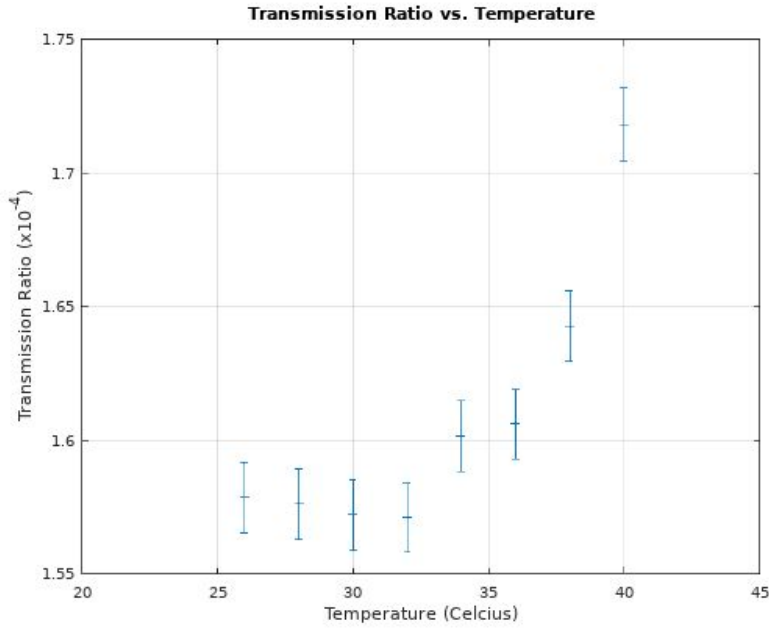
0ā ~ / ^ A F E V / a } • { ā • ā } Ū a e ĩ Á • Ę Œ \* / ^ Á a G Ū ^ \* / ^ ^ • Ę

The transmission ratio changes with temperature as so:

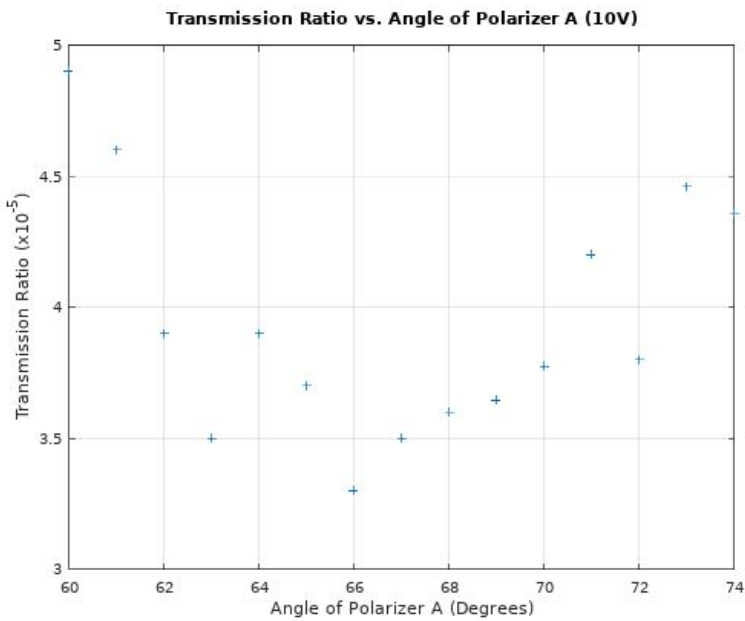


0ā ~ / ^ A F F E V / a } • { ā • ā } Ū a e ĩ Á • Ę Œ \* / ^ Á a G Ū ^ \* / ^ ^ • Ę @ Á a Á d ] • Á & / ^ a e ā \* Ę

In terms of the transmission ratio, the dependence on temperature is:



For all the transmission ratios shown above, the extinction was taken in the 0V active state as this value was about 10x the extinction of the 10V state. As such, it is of more importance to optimize the 0V state. Regardless, the 10V state will always perform better. Additionally, the transmission ratios calculated using the 10V extinction value failed to yield a convincing trend:

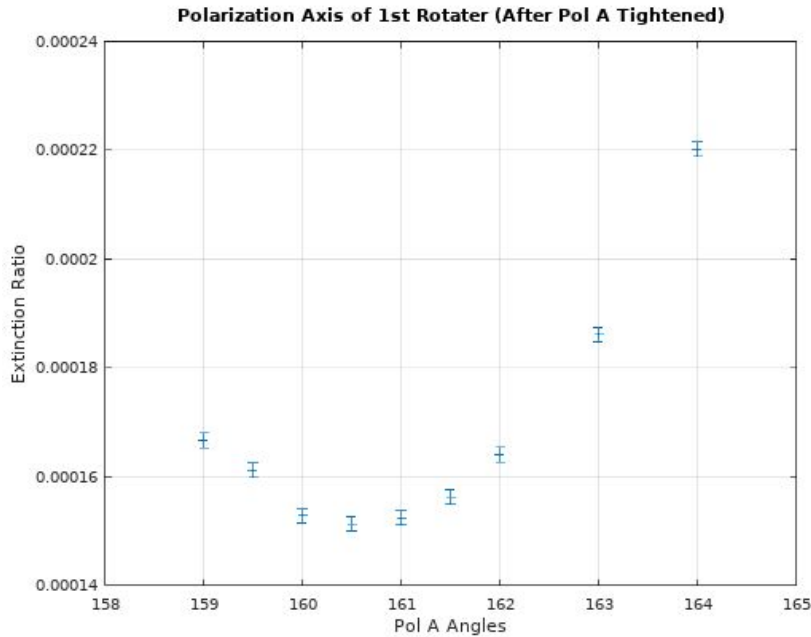


The uncertainty in the transmission ratio was calculated using the following formula:

$$\frac{\delta z}{z} = \sqrt{\left(\frac{\delta a}{a}\right)^2 + \left(\frac{\delta b}{b}\right)^2}$$

The uncertainty in angle readings is  $\pm 0.125$  degrees due to the small size of the Thorlabs CRM-1 Vernier scale on the polarizer mounts. A point grey camera was set up to magnify Pol B while Pol A was magnified by taking a picture with a cellphone camera on flash.

After tightening the first polarizer, Pol A, the new polarization axis is 160.5 degrees:

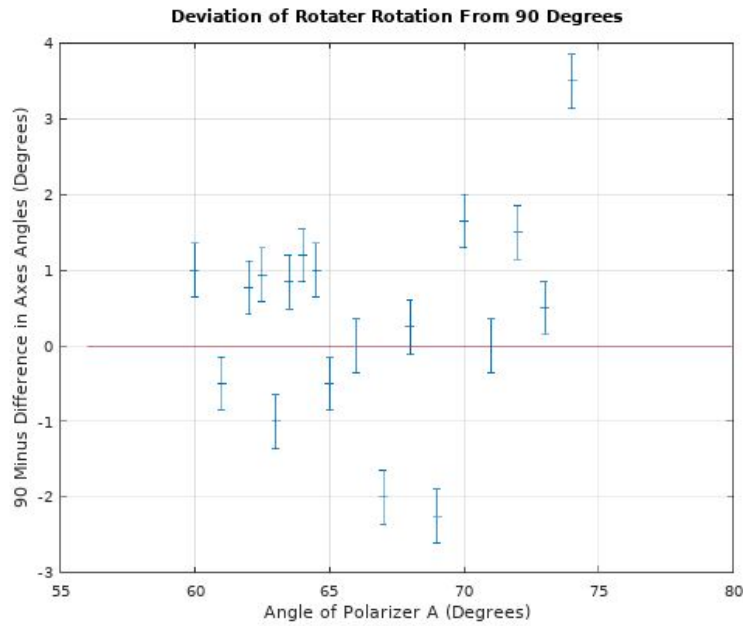


Initially, the analyzing polarizer (Pol B) was mounted too loosely, and as a result, the flipping angle deviation from 90 degrees varied from -3 to 3 degrees as shown in Figure 10. 'Creeping' of Pol B was observed to be a problem. That is, after Pol B was adjusted to the maximum extinction, the power would increase again, but only in one direction, indicating 'creeping' of Pol B in its cage.

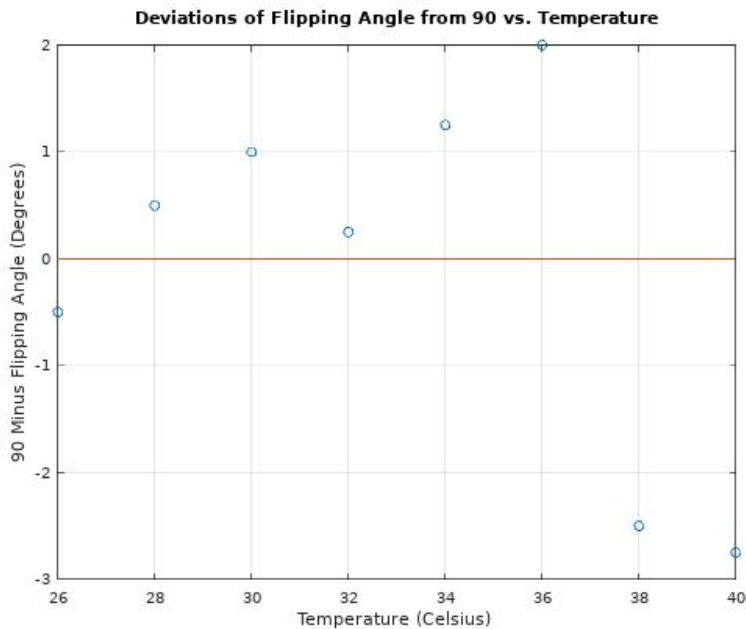
### iii. 90 Degree Flip

Initially, the analyzing polarizer (Pol B) was mounted too loosely, and as a result, the flipping angle deviation from 90 degrees varied from -3 to 3 degrees as shown in Figure 10. 'Creeping' of Pol B was observed to be a problem. That is, after Pol B was adjusted to the maximum extinction, the power would increase again, but only in one direction, indicating 'creeping' of Pol B in its cage.





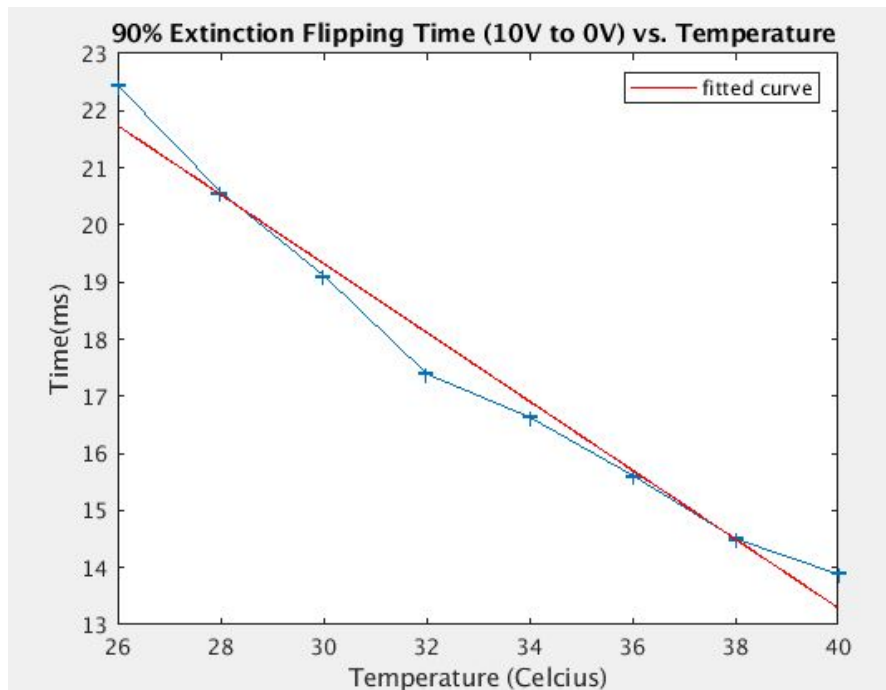
After tightening Pol B, the deviations varied only within one degree around 0 degrees, a significant improvement. Birefringence, which can occur with over-tightening, was not observed to be a problem as power levels observed after tightening were comparable to those before. The flipping angle also varied with temperature:



Though not shown explicitly in Figure 15, the uncertainty for both Figure 14 and Figure 15 was calculated by adding the angle reading uncertainties ( $\pm 0.125$ ) in quadrature, resulting in an uncertainty of  $\pm 0.18$  degrees.

#### iv. Flipping Time

The time it takes for the rotator to flip from 10V to 0V (fall), ie. the time it takes to rotate the crystals, is about 10x longer than it takes to flip from 0V to 10V (rise). Additionally, the flipping time increases with temperature. Flipping times were recorded on both the mW and the uW scale for both rise and fall. Pol B was rotated 90 degrees to extinguish the power in order to produce a decay curve on the oscilloscope for the 'rise.' Additionally, the waveform was triggered on the rising edge. The horizontal scale was centered at half the period in order to capture the 'fall' decay curve. For the 'rise' decay curve, the scale was re-centered at 0 seconds. Cursors were then used to measure the time: Horizontal cursors were placed at the maximum and at 10% of this value. Then, vertical cursors were aligned with the horizontal ones. The difference between the vertical cursors was taken to be the flipping time. The uncertainty was determined by considering the thickness of the waveform displayed. The flipping times decrease linearly with time as shown below:



Though not shown explicitly in Figure 15, the uncertainty for both Figure 14 and Figure 15 was calculated by adding the angle reading uncertainties ( $\pm 0.125$ ) in quadrature, resulting in an uncertainty of  $\pm 0.18$  degrees.





there are some variations with being turned on and off. However, the results in Figure 16 were calculated using very typical power values, that is, diode laser power values that are observed very consistently in the lab.

Using this Mueller matrix, only S1 ends up affecting the final S3 value. S2 adds a very marginal amount of ellipticity. However, this matrix is still an effective way to estimate S3 as Figure 6 confirms experimentally that S2's contribution to S3 is negligible. In other words, experimental results agree with Mueller matrix calculations.

For a best extinction of 0.35 uW and best transmission of 775 uW, the calculated S3 is 0.9991. These power values result in a transmission ratio of  $4.5 \times 10^{-4}$ , which is much worse than any experimentally observed transmission ratio. This means that although the transmission ratio gets worse after 32 degrees Celsius, the S3 is still sufficiently good.

More than S1, the biggest factor in determining S3 is the accuracy of the 45 degree angle between the maximum and minimum axes. Even small deviations from 45 result in a very poor S3. For this reason, it is advisable to operate at lower temperatures, if the flipping time is sufficient for experimental needs. For example, changing the angle to 44 degrees in the above calculation results in an S3 of 0.9981. Even when using the 10V beam values, having the wave plate at 44 degrees instead of 45 results in an S3 of 0.9983. As such, conditions should be adjusted to optimize the flipping angle in order to optimize the S3.

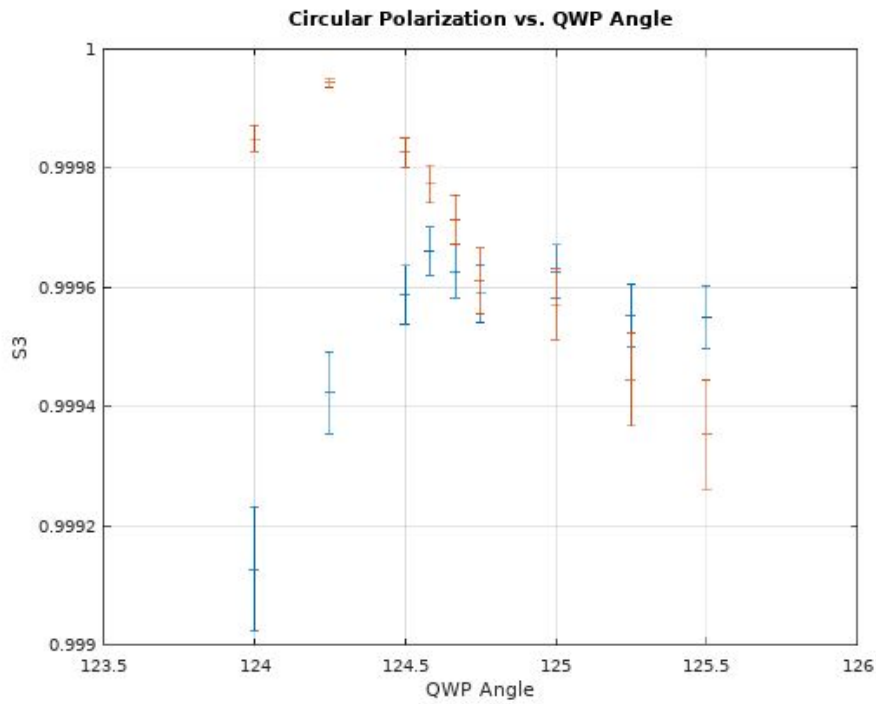
The projected S3 value for this binary rotator, even in the poorer rotated state, is about 10x better than the poorer S3 value achieved using the liquid crystal variable retarder:

	Laser port	$s_3^{in}$	$s_3^{out}$
$\sigma^-$	Upper	-0.9980(4)	-0.9958(8)
	Lower	-0.9990(10)	-0.9984(13)
$\sigma^+$	Upper	0.9931(9)	0.9893(14)
	Lower	0.9997(3)	0.9994(5)

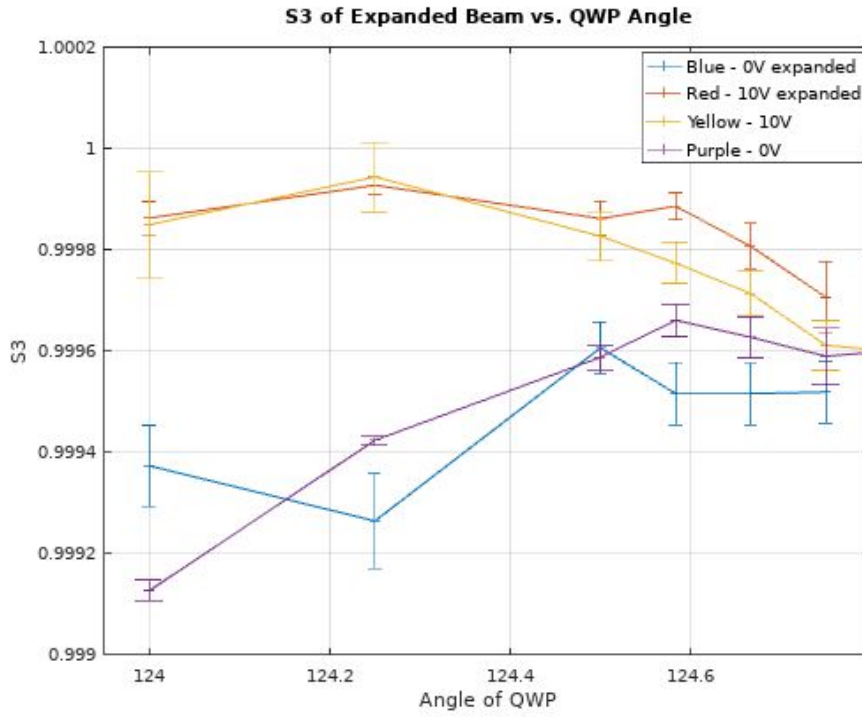
~~0a ~ ! ^ Á G G Á V @ Á | á Á ç ^ • Á | Á H á & @ ç ^ á Á • á \* Á @ Á á ~ á & ^ • ç á ç á ç | ^ Á ^ ç á ^ | B I Á~~

The fast axis of the 767nm quarter wave plate was experimentally determined in both the 0V and 10V states and angles approximately in the middle of the two axes (approximately 45 degrees from the two fast axes) were investigated, producing the result shown in Figure 19. The

maxima for the 10V state is more well defined than that of the 0V state:



$\sigma^2$  is the variance of the  $S_3$  values. The  $S_3$  values are plotted against the QWP angle. The blue data points show a clear peak at approximately 124.5 degrees, while the orange data points show a dip at the same angle. The error bars represent the uncertainty in the  $S_3$  measurements.

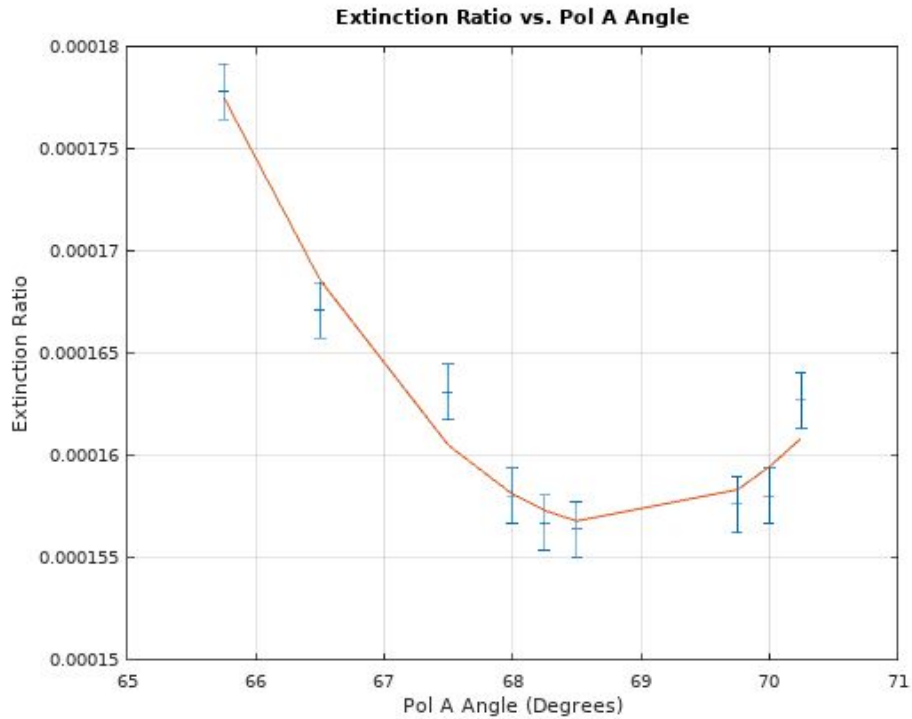


Á

0ã ~ !^Á G ÈÖç] æ åã \* Á@Á^æ Á@Á [ Á~&Á } Á@ÁHÁ

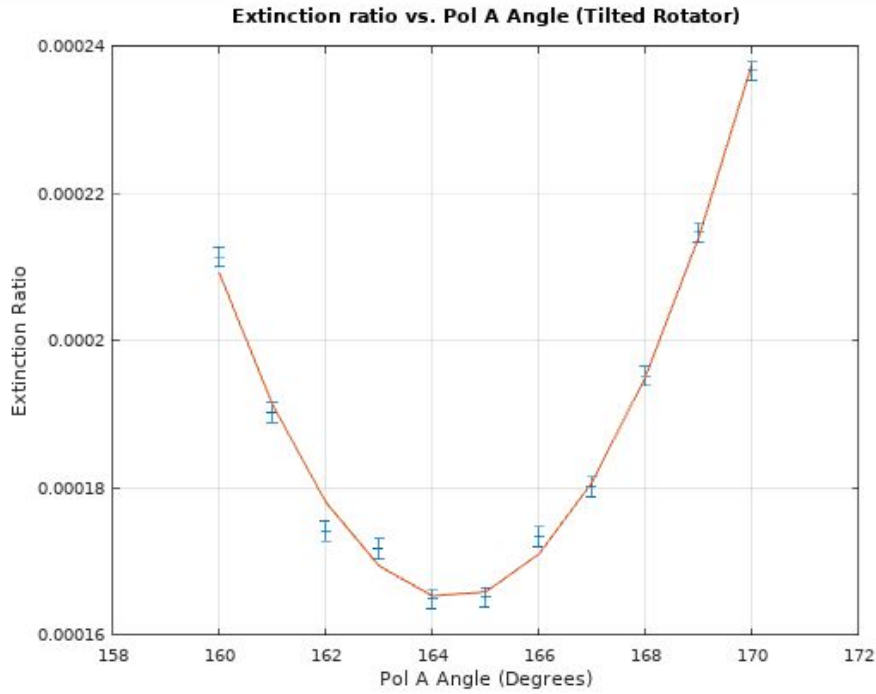
#### 4. Characterization of Second Binary Rotator

##### i. Polarization Axis

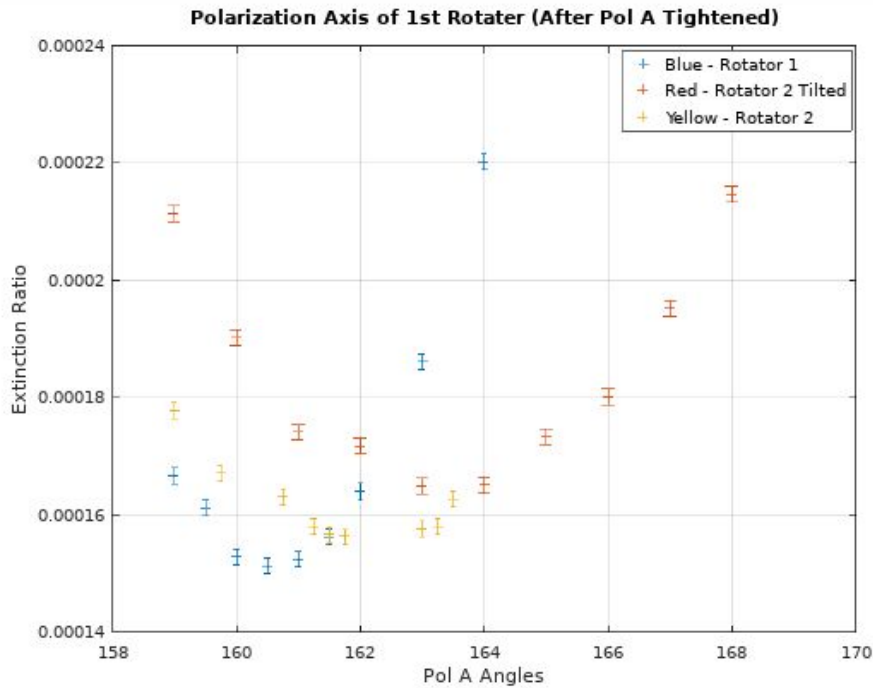


$$\begin{aligned}
 & \text{To try to correct the 92 degree flip (discussed later) by adjusting the thickness, the rotator was} \\
 & \text{tilted using an adjustable mount. Tilting the rotator caused the extinction ratio to be slightly} \\
 & \text{worse, however, the quadratic trend is more evident as shown in Figure 26.}
 \end{aligned}$$





When plotted together, the extinction ratio curves for the second rotator both have broader minimums than that of the first rotator. That is, the first rotator's curve is more steep, as shown in Figure 27.

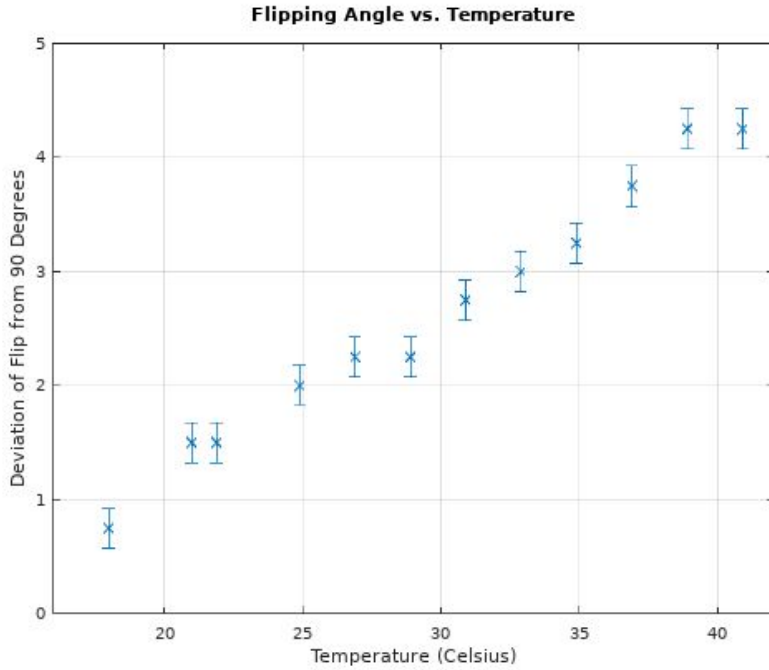


0a ~ !^AG EV @ A @ ^ A ca & q } R ~ i c ^ • A || w a A \* ^ c @ ! A a Q q | A A @ { A c c q \* A e F i J A ^ \* ! ^ ^ • E A  
 • Q, q \* A @ e A @ R ~ i c ^ • A | A @ A ^ & | } a A [ c a | A @ c ^ A | [ c a ^ i A q a ~ { • A a A q a \* A @ A [ c a | A  
 • | a @ ^ A [ ! • ^ } • A @ A c a & q } A c a E A  
 A

**ii. 90 Degree Flip**

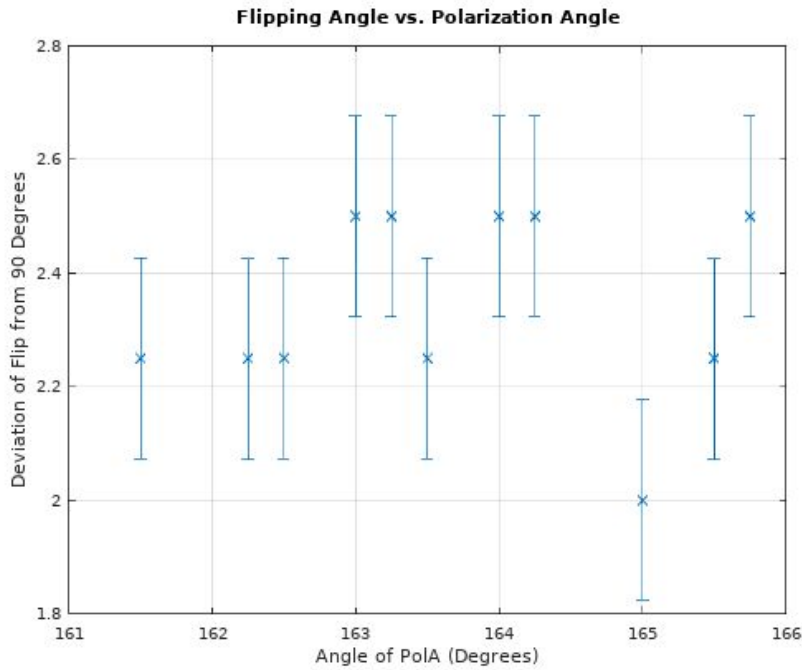
This rotator consistently has a flip of 92 to 93 degrees. In an attempt to correct the flip, the voltage was investigated. It was found that from 5V to 10V, the rotator crystals remained unrotated and the flip between the 0V state and the 5V state was still 90. Making the 0V state non-zero worsened both the flip and the extinction ratio.

Another attempt investigated the effects of temperature on the flip and found that the flipping angle increased with temperature. As such, a viable way of correcting the flip is to decrease the temperature.



0a ~ !^A G ÈV @ Á] ] ã \* Á ã \* |^Á & ^æ ^• Á ã Q { ] ^æ ^!^ È ã Q Á ^ ã \* Á È È Í Á È È Á ^ \* !^• Á Á FÌ Á ^ \* !^• Á ^ • Á ^ • Á

Incoming polarization axis was also investigated and it was found to have no effect:

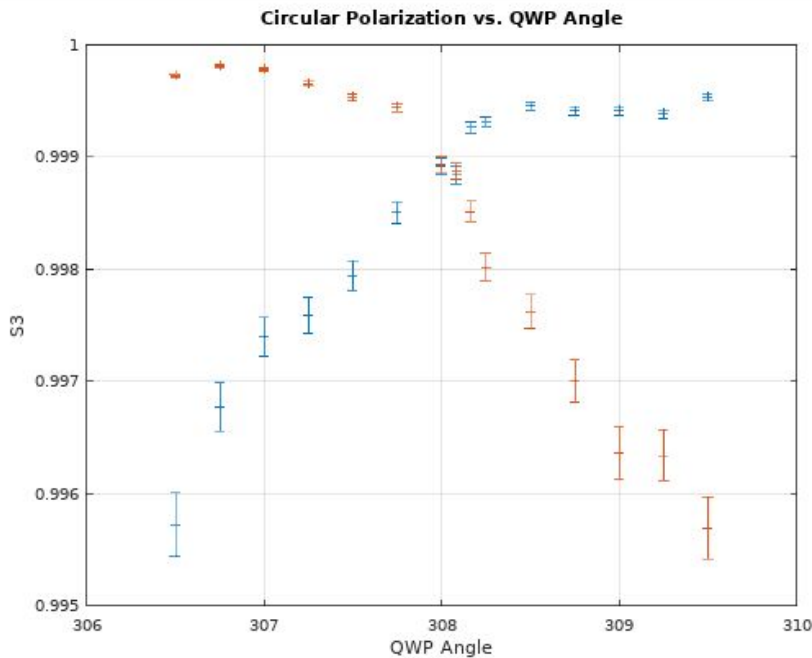


0a ~ !^A G ÈV @ Á] ] ã \* Á ã \* |^Á [ ^• Á [ o ç ^ Á ã } ã ã ã d ^ Á ã Q & { ã \* Á [ | æ ã æ ] È Á

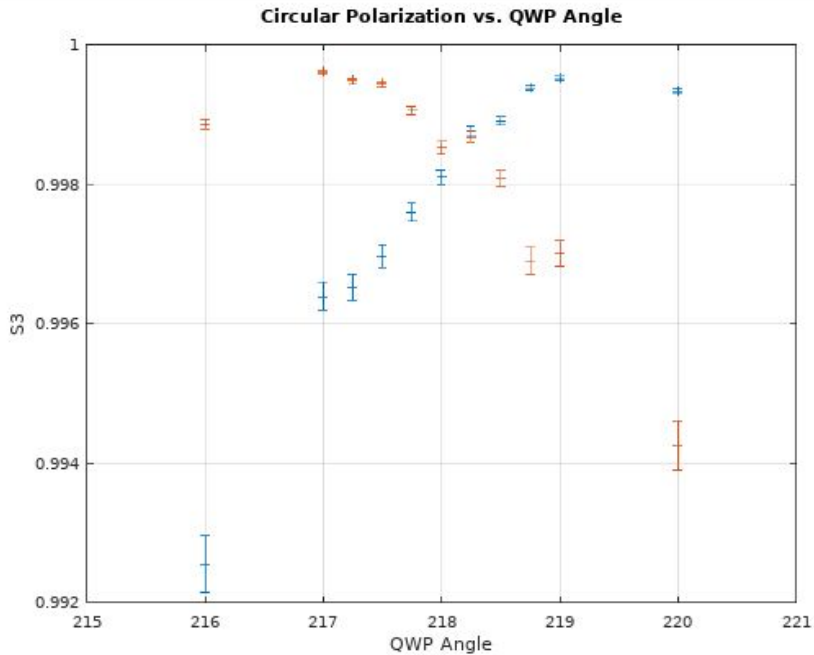
Using infrared light to look at the retro-reflected beam and confirming that the optic was properly mounted in the cage, it was determined that the actual optic is slightly tilted in its housing. Initially, it was believed that the flipping angle was correlated to the thickness of the rotator because thickness affects wave plate phase changes; however, thickness in this case had no effect. Using an adjustable mount, the manufacturer's tilt (and therefore the thickness) was corrected. However, the 92 degree flip remained.

### iii. S3 and Discussion

Due to the 92 degree flipping angle, the maxima for the 0V and 10V S3 curves do not coincide. Predictably, they are separated by about 2 degrees. While each state can achieve an S3 of over 0.9990 on its own, there is no angle at which a compromise between the states yield an S3 of over 0.9990 for both states simultaneously. The other handedness (flipping the quarter wave plate 90 degrees) was also investigated and it yielded similar results. As shown, the intersection of the two S3 curves is between 0.998 and 0.9990 for both orientations of the quarter wave plate.

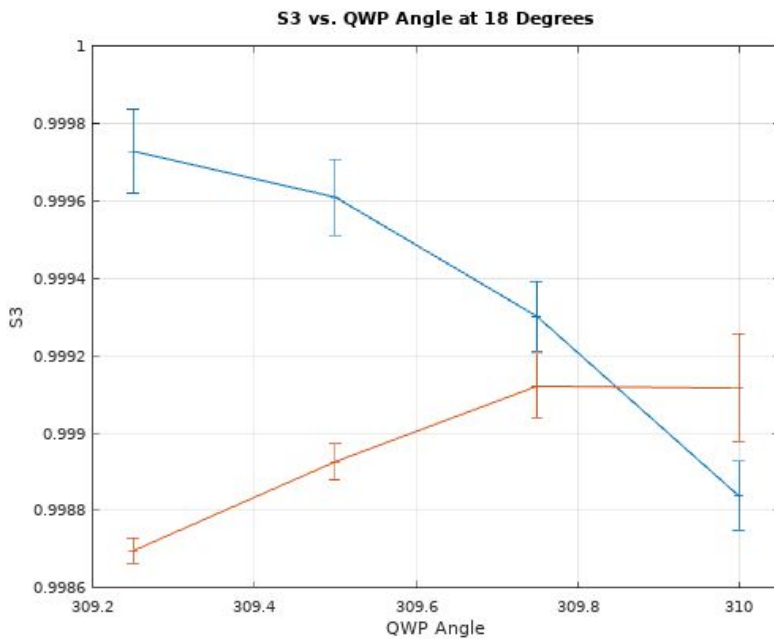


0a ~ !^AEEÜHÁ•ÉÁ ~ æc!Á æ^Á|æ^Áæ \*|^ÉÁ ã@Á@Á|^Á&|ç^Á^|!^•^} ç \*Á@ÉXÁæ^Áæ áÁ  
 c@Á!æ \*^Á&|ç^Á^|!^•^} ç \*Á@ÉXÁæ^Áæ ÉÁ



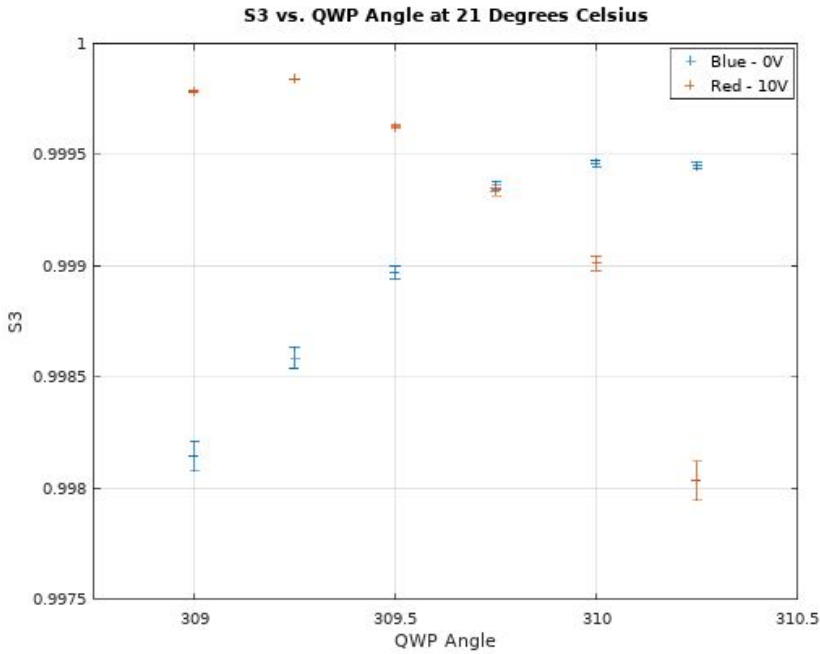
0a ~ !^A FZUHq • EÄ ~ æc!A æ^A |æ^Aq \*|^A !A @A c@!A @q â^â} ^••A A @A ~ æc!A æ^A |æ^A EÄ & } -â { â \* A @A @A XAq âA EXA^æ • Aq } [ A @A Aq UHÄ -A ç^!A EJJEA q } & EÄ

However, cooling the rotator (and the room) effectively decreased the flipping angle to 90.75 degrees, which allowed both beams to achieve an S3 of over 0.9990 simultaneously.



0a ~ !^A GZOFI A ^\* !^A • EÄ [ c@A æ • Aq } & @ ç^!Aq UHÄ -A ç^!A EJJEA q ~ |æ^! ~ • | EÄ

Á



Á

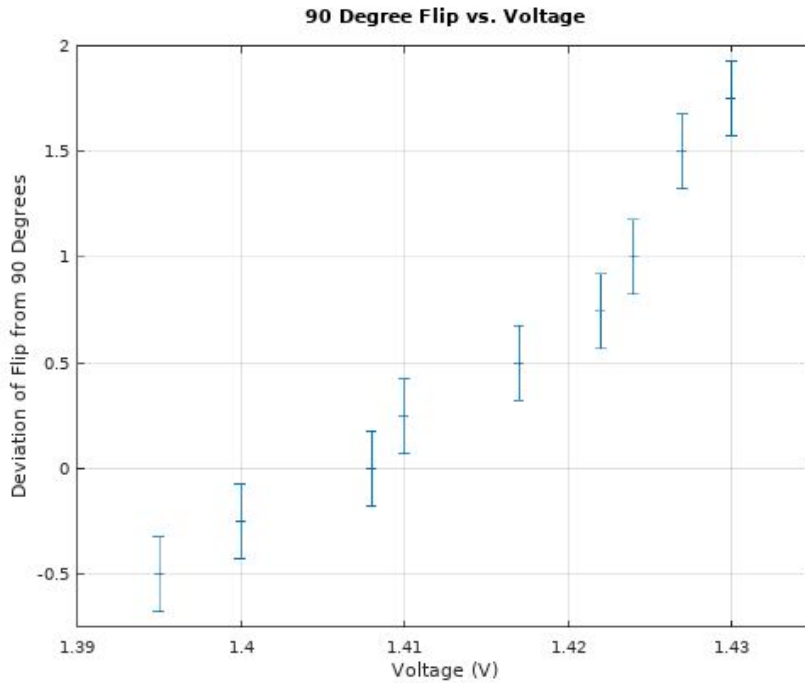
Á

0a ~ !^A HÉ05CFA ^\* !^^ • ÉaA @ Á ] a { Áa \* !^Á -ÁEJÉ | Á ^\* !^^ • Éa [ c0á aq • Áa @ Áa ÁUHA  
[ -Á Ç ! Á É U J J E Á

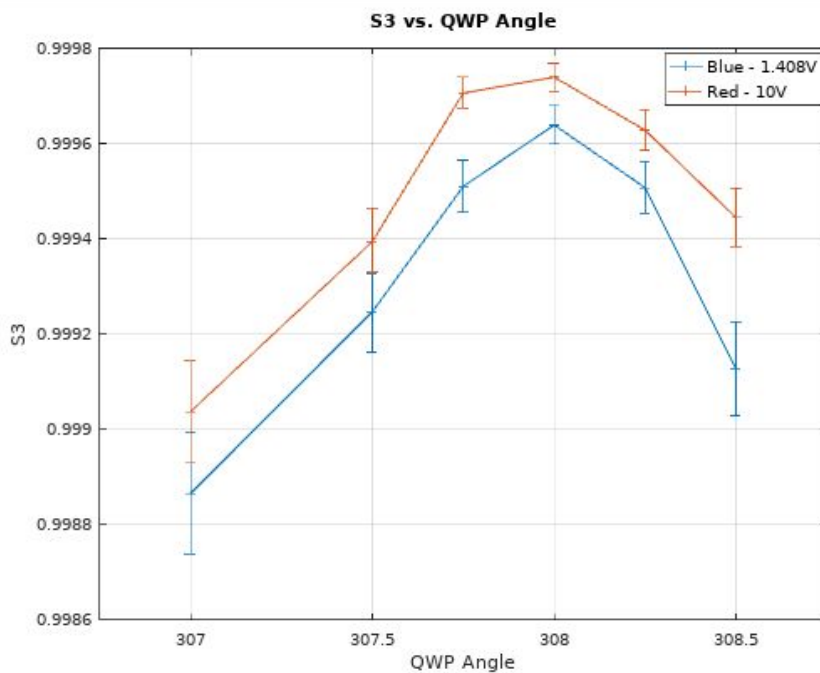
Á

#### iv. Replacement Rotator

We sent the rotator back to Meadowlark because it was not feasible to keep the rotator at a constant temperature of 18 degrees. They sent us a replacement which specified that the flip would be 90 degrees between 1.424V and 10V, however, with the ambient temperature in the lab, it was found that using 1.408V and 10V yielded a 90 degree flip more accurately. The following plot shows the dependence of flip on voltage:



Using 1.408V and 10V, the maximums of the S3 plots for both the 0V and 10V beams coincided as shown:



0a ~ !^AÍ ÈY @) Á@Áq Á Á€Á^\* !^•É@Á [ ÁUHÁ ][ • Á ^ a Á@Áæ ^Áq \*|^É  
Á

## 5. Camera Programming

### i. Dynamic Memory Allocation

In the original Acquisition.cpp example provided by the PointGrey Spinnaker software development kit, the pictures were acquired and saved to disk alternatively. That is, right after a picture was acquired, it was saved before the next picture was acquired. This slowed the acquisition rate as saving to disk takes time. With my new code, the pictures are saved after they have all been acquired. Thus, the acquisition rate is increased since pictures are not saved alternatively. I used a 'vector' in C++ to store the images instead of saving them. After acquisition, the code loops through the vector and saves the images one by one. My code also adjusts image parameters like region of interest, gain, and exposure. Hardware and software triggers can also be used with the code to control acquisition. These adjustments and functionalities were implemented using the 'Node Map' system that the new Spinnaker SDK uses. The Blackfly S technical reference [7] provides very thorough information about the node map while the examples included in the SDK demonstrate how to manipulate the nodes.

I also implemented dynamic memory allocation on the Flea3 camera by editing the provided FlyCapture2 SDK CustomImageEx.cpp example as well. I also implemented hardware triggering into the code by looking at the provided AsyncTriggerEx.cpp also from the FlyCapture2 SDK. As such, the Flycapture2 code has very similar functionality to the Spinnaker code.

After contacting them for help, PointGrey also provided a multithreaded program that also increases the acquisition rate by not alternating between acquiring and saving pictures. Their program uses one thread to acquire images and another thread to process them. Software triggering through another user-interface thread is used to control the program. However, at this point, hardware triggering is not compatible with the multithreaded code. The major difference between the multithreaded code and my code is that in the multithreaded code, image processing and image acquisition are concurrent while in my code, the images are processed afterwards.

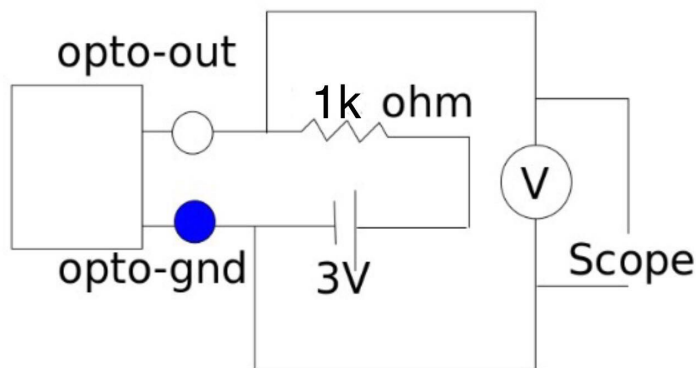
### ii. Achieving Max Frame Rate

Implementing the suggestions provided from PointGrey, I was able to achieve a maximum frame rate of 370 frames per second using both the multithreaded code they provided and my own code with the adjusted image parameters. The region of interest was set to be 200 pixels by 200 pixels. PointGrey confirmed that there is nothing else we can do to increase the frame rate further.



I was also able to achieve a frame rate of 370 frames per second on the Flea3 camera at the maximum region of interest using my Spinnaker codes, however, Claire Preston listed a much higher frame rate in her report of one frame per 1.25 microsecond using her routines. [8]

By adding a pull-up resistor circuit and an oscilloscope, the trigger pulse and the strobe response from the camera can be displayed. The strobe response rise signified the start of exposure. It was observed that the strobe response from the camera varied slightly with each acquisition. This means that the exposure start time varied within 10 microseconds from frame to frame. Changing the value of the resistor may decrease the rise time of the strobe output signal. The following circuit was used in order to achieve this functionality:



øã ~ !^Áî ËÛ ~ ||Ë ] Á^•ã ç !Á& ãÁ •^ãÁ Á^óÁ d[ à^Á ~ ç ~ óÁ [ { Á&ç ^!ãËÁ  
 Á

### iii. Information From Point Grey

The following is a summary of the information contained in the support emails recieved from PointGrey. The original emails have been forwarded.

It is impossible to use the on camera buffer to capture a short burst of images at higher than USB3 bandwidth and then transfer them to the host at USB3 bandwidth after the burst is finished. The max frame rate is based off of the USB3 bandwidth limit for this camera. Adjusting the region of interest will increase the frame rate, according to the table listed in the Blackfly S technical reference. The camera memory does have a user buffer which is capable of storing data, however it is slow and will not help in increasing the frame rate. Additionally, the User Controlled Transfer Queue mode is typically used by customers that want to capture a burst of images on multiple cameras that are sharing a single USB3 link and then have them transfer the images one camera at a time. The order in which images are saved can be adjusted by learning from the BufferHandling C++ example Spinnaker provides. Note that there are some issues with the Overwrite buffer handling modes in Ubuntu in the current production release (NewestOnly, NewestFirstOverwrite, and OldestFirstOverwrite). Upon request, PointGrey can provide a beta that has a fix for this issue. Before an image is assigned to an 'ImagePtr' and thereby allocated

space in computer RAM memory, it is stored in the host side image bugger. In other words, the ImagePtr is the first form of the camera image that can be manipulated.

From a different PointGrey representative, we found out that there is a 200 frames per second firmware cap on PointGrey cameras to ensure the auto algorithms work well. To exceed this limit, auto settings such as auto exposure, auto gain, auto white balance need to be disabled. Once all auto algorithms are disabled the 200 frames per second limit can be exceeded. I found this to be true as the frame rate increased to 370 instead of 200 for the same region of interest once the auto-algorithms were disabled. This representative also said that apart from implementing dynamic memory allocation and disabling these auto-algorithms, there is nothing else that will further increase the frame rate.

#### **iv. File List**

##### **Spinnaker SDK**

```
/home/trinat/pointgrey/spinnaker-1.20.0.14-amd64/spinnaker/src/Acquisition/  
Acquisition.cpp
```

This is the multithreaded program provided by PointGrey.

```
/home/trinat/pointgrey/spinnaker-1.20.0.14-amd64/spinnaker/src/Acquisition/  
Acquisition2.cpp
```

This is the program I wrote which utilises vectors to implement dynamic memory allocation. It is compatible with software and hardware triggers.

##### **FlyCapture2 SDK**

```
/home/trinat/flycapture/flycapture2-2.13.3.31-amd64/flycapture/src/CustomImageEx/  
CustomImageEx.cpp
```

This program has similar functionality to the Acquisition2.cpp one, but written using the FlyCapture2 SDK. It also includes functionality for hardware triggering.

## **6. Moving Forward**

### **i. Optics**

In order to better diagnose the spin-polarization of the atoms, a faster rotator could be used to polarize the atoms one way first, then the other. The current model, even at higher temperatures, is not fast enough to achieve this.

